ACS APPLIED MATERIALS & INTERFACES

www.acsami.org

Research Article

Zirconium and Aluminum MOFs for Low-Pressure SO_2 Adsorption and Potential Separation: Elucidating the Effect of Small Pores and NH_2 Groups

Philipp Brandt, Shang-Hua Xing, Jun Liang, Gülin Kurt, Alexander Nuhnen, Oliver Weingart,* and Christoph Janiak*

Cite This: *ACS Appl. Mater. Interfaces* 2021, 13, 29137−29149

Read Online

ACCESS | Metrics & More | Article Recommendations | Supporting Information

ABSTRACT: Finding new adsorbents for the desulfurization of flue gases is a challenging task but is of current interest, as even low SO_2 emissions impair the environment and health. Four Zr- and eight Al-MOFs (Zr-Fum, DUT-67(Zr), NU-1000, MOF-808, Al-Fum, MIL-53(Al), NH_2-MIL-53(Al), MIL-53(tdc)(Al), CAU-10-H, MIL-96(Al), MIL-100(Al), NH_2-MIL-101(Al)) were examined toward their SO_2 sorption capability. Pore sizes in the range of about 4−8 Å are optimal for SO_2 uptake in the low-pressure range (up to 0.1 bar). Pore widths that are only slightly larger than the kinetic diameter of 4.1 Å of the SO_2 molecules allow for multi-side-dispersive interactions, which translate into high affinity at low pressure. Frameworks NH_2-MIL-53(Al) and NH_2-MIL-101(Al) with an NH_2-group at the linker tend to show enhanced SO_2 affinity. Moreover, from single-gas adsorption isotherms, ideal adsorbed solution theory (IAST) selectivities toward binary SO_2/CO_2 gas mixtures were determined with selectivity values between 35 and 53 at a molar fraction of 0.01 SO_2 (10.000 ppm) and 1 bar for the frameworks Zr-Fum, MOF-808, NH_2-MIL-53(Al), and Al-Fum. Stability tests with exposure to dry SO_2 during ≤10 h and humid SO_2 during 5 h showed full retention of crystallinity and porosity for Zr-Fum and DUT-67(Zr). However, NU-1000, MOF-808, Al-Fum, MIL-53(tdc), CAU-10-H, and MIL-100(Al) exhibited ≥50−90% retained Brunauer−Emmett−Teller (BET)-surface area and pore volume; while NH_2-MIL-100(Al) and MIL-96(Al) demonstrated a major loss of porosity under dry SO_2 and MIL-53(Al) and NH_2-MIL-53(Al) under humid SO_2. SO_2 binding sites were revealed by density functional theory (DFT) simulation calculations with adsorption energies of −40 to −50 kJ·mol^{-1} for Zr-Fum and Al-Fum and even above −50 kJ·mol^{-1} for NH_2-MIL-53(Al), in agreement with the isosteric heat of adsorption near zero coverage (ΔH^0_{ads}). The predominant, highest binding energy noncovalent binding modes in both Zr-Fum and Al-Fum feature μ-$OH^{\delta+}\cdots^{\delta-}OSO$ hydrogen bonding interactions. The small pores of Al-Fum allow the interaction of two μ-OH bridges from opposite pore walls with the same SO_2 molecule via $OH^{\delta+}\cdots^{\delta-}OSO^{\delta-}\cdots^{\delta+}HO$ hydrogen bonds. For NH_2-MIL-53(Al), the DFT high-energy binding sites involve $NH^{\delta+}\cdots^{\delta-}OS$ together with the also present Al-μ-$OH^{\delta+}\cdots^{\delta-}OS$ hydrogen bonding interactions and C_6-$\pi^{\delta-}\cdots^{\delta+}SO_2$, $N^{\delta-}\cdots^{\delta+}SO_2$ interactions.

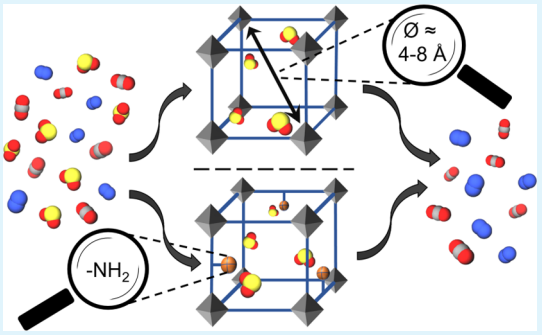

KEYWORDS: *sulfur dioxide, pore size, adsorption, metal−organic framework, flue gas desulfurization*

INTRODUCTION

A large fraction of the toxic gas sulfur dioxide (SO_2) is emitted into the atmosphere from industrial processes and fossil fuel combustion.[1] In 2018, energy-related coal combustion was accountable for 43% of SO_2 emissions worldwide.[2] SO_2 emissions are damaging to the biosphere both through the formation of acid rain and by contributing to air pollution issues, such as particulate matter (PM) with a diameter of ≤2.5 μm.[3−5]

Typically, wet limestone scrubbing or treatment by amine-based absorbents are used to remove SO_2 from flue gases. In both cases, the absorption is usually irreversible or accompanied by energy-intensive processes.[6] Calcium sulfite is the product of limestone scrubbing and is oxidized to produce flue-gas-desulfurization (FGD) gypsum, which is mainly utilized in the construction industry. Yet, lime-stone scrubbing leaves up to 150−450 ppm of SO_2, which can significantly reduce other flue gas purification processes by inactivating sorbents for CO_2 removal or catalysts for selective reduction of NO_x.[7−9] On the other hand, reversible SO_2 adsorption could be utilized in a much fruitful way by aiming at producing the industrially crucial sulfuric acid, without other by-products.[10] Dry FGD technol-

Received: April 1, 2021
Accepted: May 27, 2021
Published: June 11, 2021

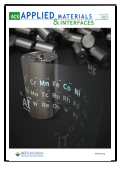

https://doi.org/10.1021/acsami.1c06003
ACS Appl. Mater. Interfaces 2021, 13, 29137−29149

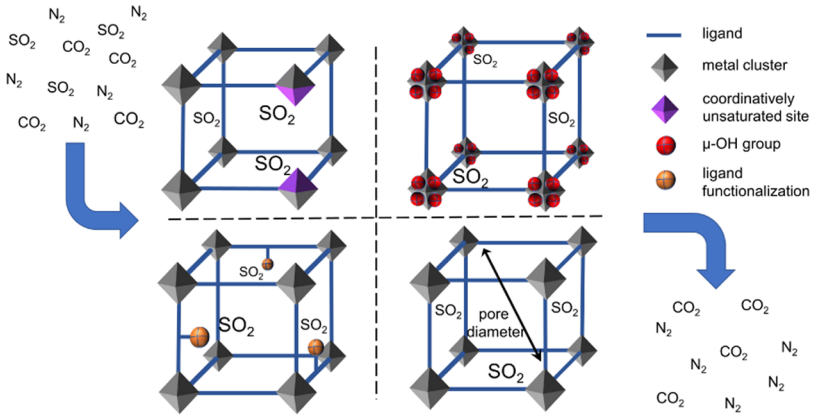

Figure 1. Schematic visualization of potential influencing factors for the low-pressure adsorption of SO_2 in porous materials.

Scheme 1. Zr- and Al-MOFs Investigated for SO_2 Adsorption[a]

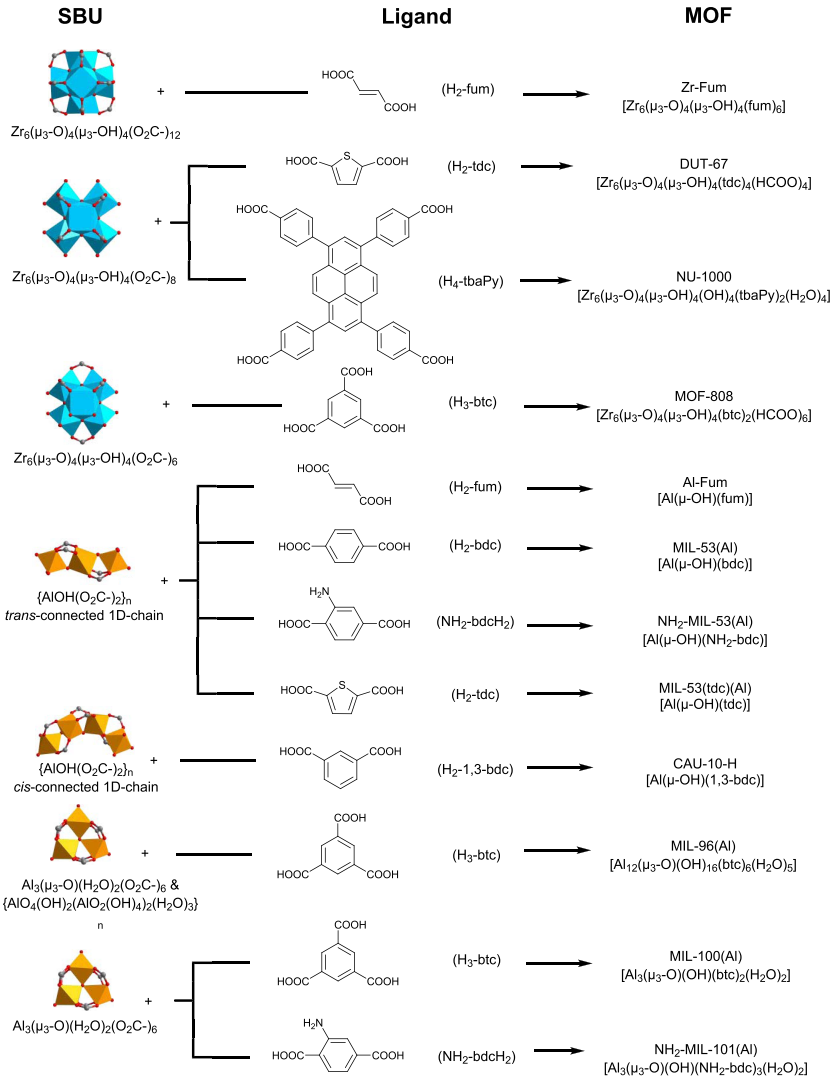

[a]Secondary building units (SBUs) depict the metal, carbon (gray), oxygen (red), and metal coordination polyhedra of Zr (cyan) and Al (orange) (left column), which are connected via the organic carboxylate ligands (acid form in the middle column) to form respective MOFs (right column).

ogies are expected to become competitive if cycling-efficient adsorbents with quantitative SO_2 removal would be available to balance the higher capital costs for a regeneration unit.[11]

Metal−organic frameworks (MOFs) represent a promising adsorbent class due to record-holding surface areas (>7000 m^2 g^{-1}) and uniform and designable porosity, typically in the microporous domain.[12] A combination of both inorganic and

https://doi.org/10.1021/acsami.1c06003
ACS Appl. Mater. Interfaces 2021, 13, 29137−29149

organic building units is the reason for the high variety and tunability of MOF materials. Owing to their high porosity, MOFs outperform competing adsorbents, like zeolites and activated carbons, leading to a considerable number of studies related to various gas storage and gas separation applications,[13−15] including the capture of toxic and polluting gases.[16−22]

Until about 8 years ago, research on SO_2 adsorption of MOFs was of specialized interest,[23−26] but recently has experienced a surge of attention.[27−32] For example, MFM-300(Al) and MFM-601(Zr) showed promising results for selective SO_2 adsorption and outstanding robustness.[33−35] Previously, we had examined MIL-160(Al), which exhibited an excellent ideal adsorbed solution theory (IAST) selectivity of 128 at 293 K and 1 bar for SO_2/CO_2 gas mixtures (10:90 v/v).[36]

For the use of MOFs in the selective adsorption of SO_2 traces below 500 ppm, the low pressure (p < 0.01 bar) SO_2 uptake is more relevant compared to the overall capacity reached at ambient pressure. Currently, the designed synthesis of porous adsorbents for highly selective removal of SO_2 from flue gas is still challenging and more endeavors are necessary to elucidate the underlying principles for optimal MOF SO_2 adsorbents. A model of potential factors influencing the selective SO_2 adsorption of an adsorbent is visualized in Figure 1.

So far, it is still a matter of discussion as to which factors constitute high SO_2 uptakes at low pressures (p < 0.01 bar).[37] In this work, we elucidate small pore widths and NH_2-substituents as critical MOF parameters to achieve high quantities in low-pressure SO_2 adsorption by focusing on Al- and Zr-MOFs, which are generally regarded as rather hydrothermally stable.[38−41] Also the determination of IAST-selectivities for SO_2/CO_2 gas mixtures provides a first indication for the separation performance of a given material. Overall, the results should allow designing MOFs to remove low SO_2 concentrations from $N_2/CO_2/SO_2$ gas mixtures.

EXPERIMENTAL SECTION

Materials and Methods. All reagents were purchased from commercial vendors and used without further purification. The MOFs were synthesized according to the published literature or were purchased (Table S1). The MOF identity was established by positively matching the powder X-ray diffractograms (PXRD) with the simulation from published cif-structure files and by a porosity analysis of the nitrogen sorption isotherms (see the Supporting Information for details).

Powder X-ray diffraction (PXRD) measurements were performed on a Bruker D2 Phaser with a Cu Kα-cathode source (λ = 1.54182; 30 kV, 10 mA) at room temperature. The finely ground samples were measured in the 5° < 2θ < 50° range at a scan rate of 40 s deg^{-1} using a flat, low background silicon sample holder. N_2 gas adsorption for the Brunauer−Emmett−Teller (BET) surface area and porosity characterization was performed on a Quantachrome Autosorb 6 automatic gas adsorption analyzer. This instrument is not optimized to analyze very small micropores, and hence, a small number of data points are seen in the N_2 sorption isotherms in Figures S22−S33. At the same time, the MOFs in this work are already well characterized from the literature, and we note that our BET surface area and pore volume results agree very well (within experimental error) with the literature values. SO_2 and CO_2 sorption isotherms were measured on a Quantachrome Autosorb iQ MP.

Before each gas sorption experiment, the samples were activated according to the literature (≤3 h of degassing at ≤393 K and a ~5 × 10^{-3} mbar vacuum). The gases (He, N_2, SO_2, CO_2) were of ultrahigh purity (99.999%). The standard temperature and pressure (STP) volumes at 293.15 K and 101.325 kPa are reported in all cases according to the recommendation of the National Institute of Standards and Technology (NIST). The N_2 adsorption experiments were performed within a pressure range of 0.005−1 bar at 77 K, the SO_2 sorption experiments from 0.001 to 1 bar (0.95 ± 0.007 bar) at 293 K, and CO_2 sorption experiments from 0.001 to 1 bar (0.95 ± 0.005 bar). A Dräger Pac 6000 electrochemical SO_2 sensor with a measuring range of 0.1−100 ppm was used for leakage testing and maintaining safe work conditions.

RESULTS AND DISCUSSION

Four Zr- and eight Al-MOFs were investigated in this work and are presented in Scheme 1. Structural details are given in Section S2. The SO_2 sorption isotherms of these 12 MOFs were measured volumetrically up to 0.96 bar at 293 K. For clarity in the presentation of the SO_2 sorption isotherm diagrams, we will discuss Zr-MOFs and Al-MOFs separately.

SO_2 Adsorption by Zr-MOFs. All of the four representative Zr-MOFs have Zr_6 nodes albeit with different ligand connectivity numbers of 12, 8, or 6 for Zr-Fum, DUT-67(Zr), and NU-1000 or MOF-808, respectively.

Zr-fumarate (Zr-Fum) shows a good SO_2 affinity, already at 0.11 bar, with an SO_2 uptake of 3.1 mmol·g^{-1}, which increases to a maximum of 4.9 mmol·g^{-1} at 1 bar (Figure 2). MOF-808 and

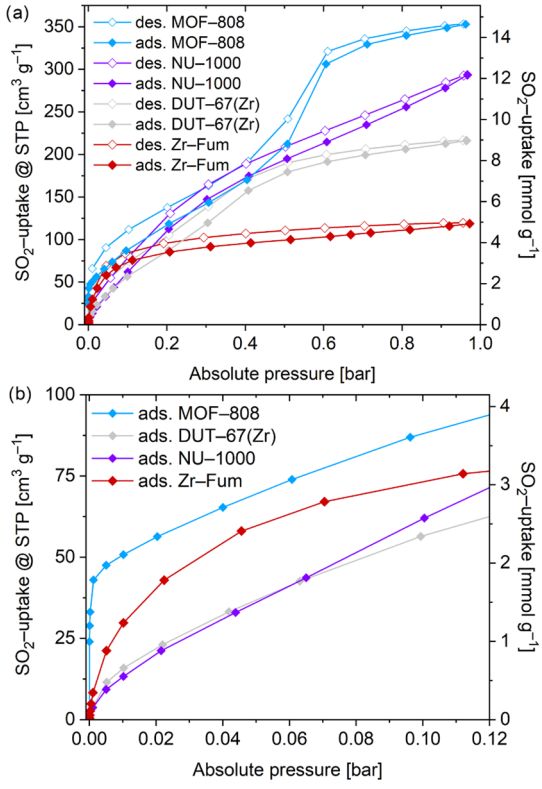

Figure 2. SO_2 sorption isotherms (293 K) of examined Zr-MOFs: (a) 0.001−1 bar and (b) 0.001−0.12 bar.

DUT-67(Zr) both exhibit two-step SO_2 adsorption isotherms (Figure 2a). In MOF-808, the first adsorption step finishes at 0.01 bar with an SO_2 uptake of 2.1 mmol·g^{-1}, followed by a moderate uptake in the pressure range of 0.01−0.5 bar up to 8.8 mmol·g^{-1}. The second step ends at 0.6 bar with an SO_2 uptake of 12.7 mmol·g^{-1}, followed by a saturation stage with a maximum of 14.6 mmol·g^{-1} at 1 bar.

Both DUT-67(Zr) and Zr-MOF NU-1000 exhibit moderate SO_2 adsorption capabilities in the low-pressure range with SO_2 uptakes of 0.7 and 0.6 mmol·g^{-1} at 0.01 bar as well as 2.3 and 2.6

https://doi.org/10.1021/acsami.1c06003
ACS Appl. Mater. Interfaces 2021, 13, 29137−29149

Table 1. Characteristics of Examined Materials in this Work and the Results of SO_2 Adsorption at 293 K

material	BET-surface area[d] [$m^2\ g^{-1}$]	total pore volume[d] [$cm^3\ g^{-1}$]	pore width[d] [Å]	SO_2 uptake [$mmol \cdot g^{-1}$] at 0.01 bar	0.1 bar	1 bar	SO_2/CO_2 IAST selectivity[d] at SO_2/CO_2 molar ratio 0.01[d]	0.1[d]	0.5[d]
Zr-Fum	600	0.290	4.8; 5.6; 7.4[42]	1.2	3.1	4.9	53	46	41
MOF-808	1990	0.749	4.8; 18.4[42]	2.1	3.6	14.6	48	66	370
DUT-67(Zr)	1260	0.544	8.8; 16.6[42]	0.7	2.3	9.0	22	22	37
NU-1000	1740	1.196	12; 29[43]	0.6	2.6	12.2	16	17	22
MIL-53(Al)	1450	0.706	8.5[e44]	0.4	3.3	10.5	17	22	43
NH_2-MIL-53(Al)	620	0.358	7.3[45]	2.0	4.3	8.0	41	42	56
Al-Fum	970	0.447	5.8[46]	1.0	4.1	7.5	34	35	36
MIL-53(tdc)(Al)	1000	0.415	8[47]	0.6	5.0	6.9	24	48	83
CAU-10-H	600	0.258	6[48]	1.2	3.7	4.8	29	27	25
MIL-96(Al)	530	0.237	~4; ~11, 11[49]	1.2	3.7	6.5	7	7	8
MIL-100(Al)	1890	0.824	25; 29[50]	0.4	2.5	16.3	17	18	38
NH_2-MIL-101(Al)	1770	1.001	25; 34[51]	1.5	3.6	17.3	29	20	16

[a]Ideal adsorbed solution theory (IAST) selectivity at 1 bar. See Section S4 for the CO_2 sorption data. [b]BET surface areas were calculated from five adsorption points of N_2 adsorption isotherm data within $0.05 < pp_0^{-1} < 0.2$. Values were rounded with the estimated standard deviation ± 50 $m^2\ g^{-1}$. [c]Total pore volumes were calculated from the experimental N_2 sorption data at $0.85 < pp_0^{-1} < 0.95$, depending on the isotherm shape. For details, see Section S3.3. [d]Pore widths as given in the literature. [e]Large pore form.

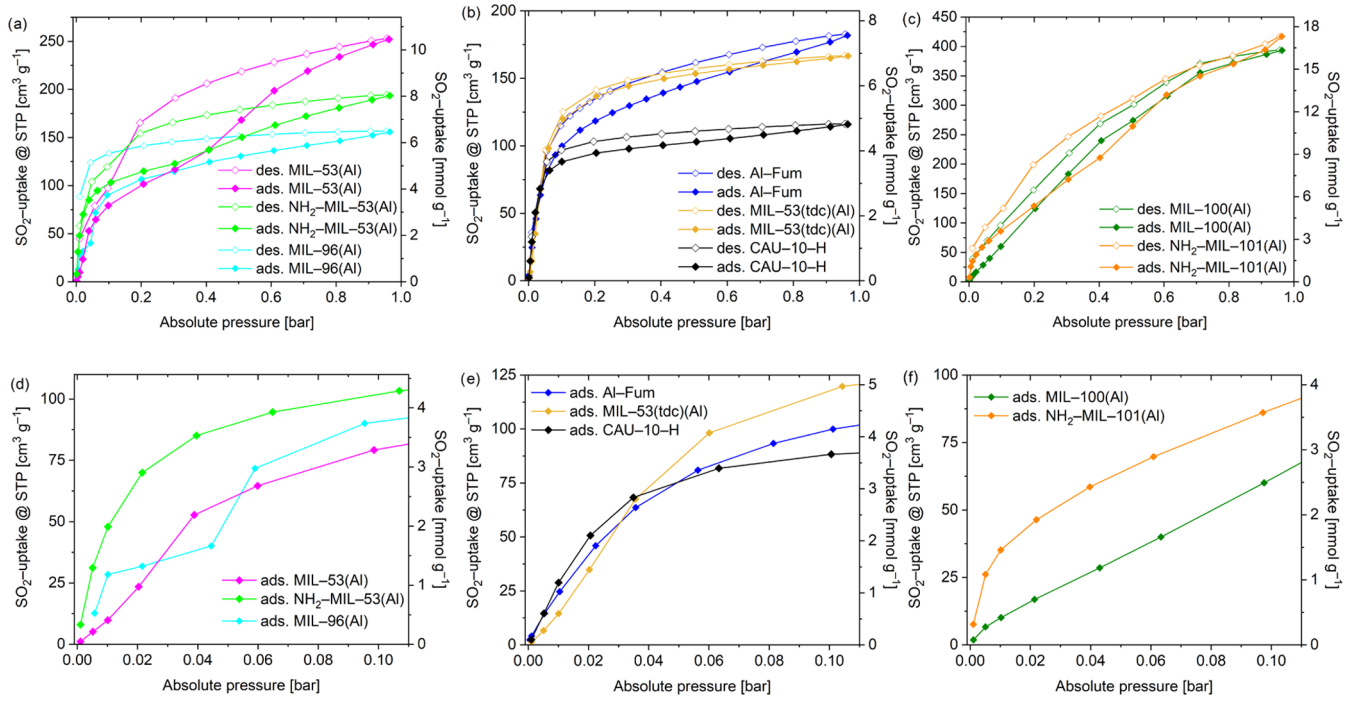

Figure 3. SO_2 sorption isotherms (293 K) of examined Al-MOFs: (a–c) 0.001–1 bar and (d–f) 0.001–0.11 bar.

$mmol \cdot g^{-1}$ at 0.1 bar, respectively (Table 1). DUT-67(Zr) shows a slight adsorption step at ~0.3 bar and a further increase until a maximum SO_2 uptake of 9.0 $mmol \cdot g^{-1}$. The SO_2 adsorption isotherm of NU-1000 increases rather steadily with a maximum SO_2 uptake of 12.2 $mmol \cdot g^{-1}$ at 1 bar and 293 K (in agreement with the isotherm in ref 52). The saturation uptake could not be reached in NU-1000 due to its micro- and mesoporosity with pore diameters of ~12 and ~29 Å for the triangular and hexagonal pore cross sections, respectively.[43]

Although all four Zr-MOFs have a bi- or multimodal pore size distribution (Table 1), we assign the observation of a two-step SO_2 adsorption in MOF-808 and DUT-67 to the simultaneous smaller (4.8 and 8.8 Å) and larger (16.6 and 18.4 Å) micropore diameters in the frameworks.[42] The two MOFs, Zr-Fum and MOF-808, with a significantly higher low-pressure uptake feature an equally smallest pore width (both 4.8 Å). The smaller pore width of DUT-67(Zr) is 8.8 Å and that of NU-1000 is 12 Å.[42] For a high low-pressure SO_2 adsorption, this suggests an optimal pore diameter of ~4 to <8 Å, as will be further discussed in the Porosity–Adsorption Relationships section.

SO_2 Adsorption by Al-MOFs. The eight representative Al-MOFs differ in their pore structures with 5 out of 8 having square to rhombic channels and infinite-chain SBUs. The infinite building units (here the Al-μ-OH-chain) and thus the resulting MOFs are known to show better thermal stability in comparison to frameworks with the same metal ions and the type of ligand but with discrete building units.[53]

https://doi.org/10.1021/acsami.1c06003
ACS Appl. Mater. Interfaces 2021, 13, 29137–29149

The Al-MOFs, MIL-53(Al), NH_2-MIL-53(Al), Al-Fum, MIL-53(tdc)(Al), and CAU-10-H, have one-dimensional channels with nearly square to rhombic cross sections of 5.8−8.5 Å. MIL-53(Al) and NH_2-MIL-53(Al) differ from the other MOFs by their reversible breathing behavior with the adsorption of guest molecules.[44,54] The complex structure of MIL-96(Al) consists of an isolated, not accessible pore A and "zig-zag" channels connecting the larger B and the smaller pore C.[49,55] MIL-100(Al) and NH_2-MIL-101(Al) have 3D pore networks of spherical mesopores of diameter ≥25 Å connected by smaller windows.

The SO_2 adsorption isotherms of MIL-53(Al) and NH_2-MIL-53(Al) (Figure 3a,d) show SO_2 uptakes to 3.3 and 4.3 mmol·g^{-1}, respectively, at 0.1 bar, which is followed by a flattening of the adsorption. Noteworthy is the rather steep increase for NH_2-MIL-53(Al) up to 0.01 bar, which will be discussed together with NH_2-MIL-101(Al). Further at 0.3−0.4 bar, both frameworks show second adsorption steps, which lead to maximum SO_2 uptakes of 10.5 and 8.0 mmol·g^{-1} at 1 bar for MIL-53(Al) and NH_2-MIL-53(Al), respectively. As mentioned above, this second adsorption step can be explained by a structure transition (breathing) from a narrow pore (np) into a large pore (lp) form, which significantly enhances the accessible space within the frameworks. The pronounced hysteresis observed in both desorption isotherms is additional evidence for phase transitions.

Previously, Liu et al.[23] and Yang et al.[56] have reported reversible phase transition upon SO_2 capture of the frameworks FMOF-2 and MFM-520, respectively. In FMOF-2, the transition can be described as a breathing mechanism, whereas, for MFM-520, an unexpected periodic-to-aperiodic structure transition was observed.

The SO_2 isotherm of MIL-96(Al) (Figure 3a,d) features two distinct adsorption steps in the low-pressure range (up to 0.1 bar). The first step finishes at 0.01 bar with an SO_2 uptake of 1.2 mmol·g^{-1}, followed by a second step starting at 0.05 bar with an SO_2 uptake of up to 3.7 mmol·g^{-1} at 0.1 bar followed by a saturation stage with a maximum SO_2 uptake of 6.5 mmol·g^{-1} at 1 bar. The stepwise adsorption reflects the complex pore structure of MIL-96(Al), which exhibits an isolated cavity A with a diameter of 11 Å and two further cavities B ∼ 11 Å and C ∼ 4 Å, which are connected and form zig-zag channels.[49] The type H2 desorption hysteresis is further evidence of a more complex pore structure in which network effects are important. The very steep desorption branch, which is a characteristic feature of H2(a) loops, can be attributed either to pore-blocking/percolation in a narrow range of pore necks or to cavitation-induced evaporation.[57]

Further, we investigated Al-MOFs with similar channel structures to MIL-53(Al), albeit more rigid, that is, without an established breathing behavior and of nearly square cross section. The SO_2 adsorption isotherms of Al-Fum, MIL-53(tdc)(Al), and CAU-10-H (Figure 3b,e) feature a similar behavior for the low-pressure range with SO_2 uptakes of 4.1, 5.0, and 3.7 mmol·g^{-1} at 0.1 bar and maximum uptake of 7.5, 6.9, and 4.8 mmol·g^{-1} at 1 bar, respectively.

CAU-10-H is isostructural to previously investigated MIL-160, which showed promising properties for a potential application in FGD processes.[36] Our results for CAU-10-H are consistent with the work reported recently by Alejandre et al.[58] The low-pressure range, up to 0.1 bar, covers 76% of the total uptake capacity in the case of CAU-10-H, which would be beneficial for pressure swing adsorption.

SO_2 adsorption in MIL-100(Al) and NH_2-MIL-101(Al) (Figure 3c,f) takes place over the whole pressure range without reaching the saturation stage at 1 bar, similar to NU-1000 (Figure 2). Again, this is due to the large pore sizes in the mesopore region. In the absence of smaller micropores, MIL-100(Al) shows one of the lowest SO_2 adsorptions at low pressures; however, with increasing pressure, it surpasses most materials examined in this work, with a total capacity of 16.3 mmol·g^{-1} at 1 bar.

The amino-functionalized MOF NH_2-MIL-101(Al) shows an initial steep increase up to ∼0.01 bar, very similar to NH_2-MIL-53(Al) (Figure 3d,f). An enhanced SO_2 uptake at low pressures was seen with amino functionalization for both NH_2-MIL-53(Al) and NH_2-MIL-101(Al) compared to their closely related frameworks, MIL-53(Al) and MIL-100(Al), respectively (Figure 3c,f). This early increase in uptake of the two NH_2-functionalized MOFs is much steeper than what is seen in this pressure range for the other Al-MOFs (cf. Figure 3d−f), which suggests its origin in the NH_2 group. This is in agreement with similar observations for the MOFs NH_2/-MIL-125(Ti)[59] and also coincides with findings for NH_2-UiO-66 exhibiting higher heat of adsorption values near zero coverage and a higher SO_2/CO_2 selectivity, compared to the parent UiO-66.[60] From a simulation of mmen-MIL-101(Cr) (mmen = *N*,*N*′-dimethylethylenediamine), the SO_2 adsorption sites were found to be transferred from Cr(III) in MIL-101(Cr) to the NH-amino groups. The lone-pair electrons from N interact with the S(SO_2) atom that has a partial positive charge. The mmen-NH groups form hydrogen bonds to O(SO_2), of the same SO_2 molecule, with distances of 1.92 and 2.27 Å as the predominant adsorption site.[61]

One gram of NH_2-MIL-53(Al) and NH_2-MIL-101(Al) corresponds to 4.5 or 1.5 mmol of the formula unit, respectively (cf. formula unit in Scheme 1) or to 4.5 mmol NH_2-bdc. Thus, at 0.01 bar, when the SO_2 uptake slope decreases, the ratios are ∼2 SO_2/4.5 NH_2-bdc in NH_2-MIL-53(Al) and ∼1.5 SO_2/4.5 NH_2-bdc in NH_2-MIL-101(Al). This suggests that two adjacent NH_2-groups can bind one SO_2 through two NH···OSO···HN hydrogen bonds in a high-affinity site. For NH_2-MIL-101(Al), the SO_2 uptake passes 3.6 mmol·g^{-1} at 0.1 bar and continues with relatively steady adsorption and reaches, albeit at no saturation yet, a maximum uptake of 17.3 mmol·g^{-1} at 1 bar, which is one of the highest reported in the literature (for a comprehensive compilation of literature data regarding SO_2 adsorption in MOFs, see Table S8). Ibarra et al. have recently investigated SO_2 adsorption in MIL-101(Cr) in which the bdc ligand was partially substituted with tetrafluoro-1,4-benzenedicarboxylate (4F-bdc) and showed a roughly similar isotherm shape to the isoreticular NH_2-MIL-101(Al) but with slightly higher SO_2 adsorption capacity with SO_2 uptakes of 4.6 and 18.4 mmol·g^{-1} at 0.1 and 1 bar, respectively, at 298 K and featured exceptional stability against SO_2.[62]

We do not see an effect of aqua ligands at the SBU for an enhanced SO_2 uptake at low pressure since MIL-100(Al) and NH_2-MIL-101(Al) with the same $\{Al_3(\mu_3\text{-}O)(OH)\text{-}(H_2O)_2(O_2C\text{-})_6\}$ SBU behave quite differently (Figure 3f). The former has the lowest SO_2 uptakes of up to 0.1 bar of all Al-MOFs. This is not to say that there would be no effect of aqua ligands or adsorbed water for other things being equal.

Ibarra et al. could observe enhanced SO_2 adsorption in the MFM-300 series related to small amounts of pre-adsorbed EtOH.[28] Also, Li et al. predicted enhanced SO_2 adsorption for MIL-160 with 0.3% pre-absorbed water.[63]

https://doi.org/10.1021/acsami.1c06003
ACS Appl. Mater. Interfaces 2021, 13, 29137−29149

The terminal metal-OH and metal-bridging μ/μ_3-OH-groups can also significantly contribute to the SO_2 adsorption performance since these groups enter in hydrogen bonding/electrostatic interactions with SO_2 (M-$O^{\delta-}$–$H^{\delta+}$···$O^{\delta-}$═$S^{\delta+}$═$O^{\delta-}$)[28,33,36,62] In our chosen Zr- and Al-MOFs, all examples feature these OH groups. In situ inelastic neutron scattering and density functional theory (DFT) calculations on the SO_2 adsorption in MFM-300(Al)[33] and in situ synchrotron PXRD studies for SO_2 in MFM-601(Zr)[64] revealed metal-OH···O═S═O hydrogen bonds for the first adsorbed SO_2 molecules. Other than that, the effect of μ-OH-groups regarding SO_2 adsorption is rarely examined in the literature. In the DFT Calculations section, we present potential binding sites of SO_2 in the representative MOFs, Zr-Fum and Al-Fum, which affirm the significant contribution of metal-OH···O═S═O interactions.

Porosity–Adsorption Relationships. The accessible surface area and the total accessible pore volume are often taken as the two prime MOF characteristics governing gas adsorption. Plots of the SO_2 uptake at 1 bar against the BET-surface area and pore volume (Figure 4a,b) show a reasonably linear correlation

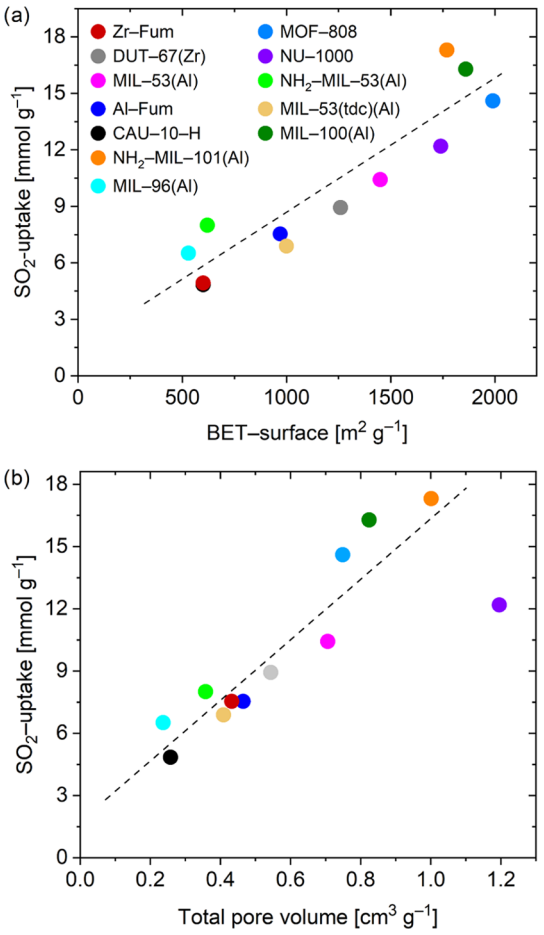

Figure 4. SO_2 uptake (1 bar, 293 K) vs (a) BET-surface area and (b) total pore volume. The dashed line is a trend line as a guide to the eye.

for most MOFs. Noteworthy outliers in the surface area correlation are NH_2-MIL-101(Al), MIL-100(Al), and NH_2-MIL-53(Al) with a higher than expected uptake based on the surface area. For NH_2-MIL-101(Al) and MIL-100(Al), their high total pore volume from micro- and mesopores gives rise to the higher uptake. The higher than expected SO_2 uptake for the flexible MOF, NH_2-MIL-53(Al), may be traced to a different extent of breathing with SO_2 at 293 K and N_2 at 77 K (where the latter yielded the accessible surface area and pore volume).

An outlier to significantly lower uptake in the uptake–pore volume relation is the Zr-MOF NU-1000, which has the highest total pore volume, even more than MIL-100(Al) and NH_2-MIL-101(Al), and is predominantly mesoporous. N_2 sorption studies with *t*-plot analysis yielded micro-to-total pore volume ratios ($cm^3\ g^{-1}/cm^3\ g^{-1}$) of 0.21/1.20 for NU-1000, 0.55/0.82 for MIL-100(Al), and 0.61/1.00 for NH_2-MIL-101(Al) (Table S2). The total pore volume represents a limit for the maximum capacity but the SO_2 adsorption isotherm of NU-1000 at 1 bar still has a high positive slope and is far from leveling off, which indicates an adsorption curve far from saturation, which will be reached only at higher pressures. Evidently, a primarily mesoporous material can be positioned below the linear trend line of the uptake–total pore volume dependence.

However, flue gas desulfurization or SO_2 gas sensors operate at low partial pressures of SO_2. When it comes to the desired high uptake at low pressure, there is no longer a surface area or total pore volume correlation. The low-pressure uptake at 0.01 and 0.1 bar is clearly independent of surface area (Figure S35). Instead, the uptake and isotherm characteristics in the low-pressure region (Figure S34) must be correlated with the SO_2 affinity of the materials. By fitting the SO_2 adsorption isotherms with an appropriate model, the affinity constants can be obtained (Table S3 and Figures S39–S50). A high-affinity constant between the adsorbent and the adsorbate reflects a high gas uptake at low pressure, which is a type-I isotherm.

When the surface-specific SO_2 uptake, that is, the uptake at low pressures (0.01 and 0.1 bar) divided by the BET-surface area, is plotted against the pore limiting diameter (PLD), an obvious maximum is obtained (Figure 5). The surface-specific

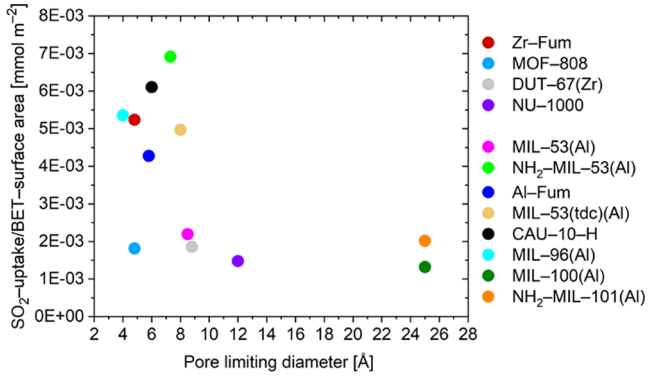

Figure 5. Surface-specific SO_2 uptake at 0.1 bar (293 K), which is the uptake at this pressure divided by the BET-surface area vs the pore limiting diameter (PLD). See Figure S36 for the surface-specific SO_2 uptake at 0.01 bar.

SO_2 uptake is obtained by normalization, i.e., division of the uptake through the surface area, which is necessary as the absolute value of the uptake at low pressure depends on the available surface area. The PLD is defined as the smallest diameter of a pore or pore window in a framework. The maximum of low-pressure uptake vs PLD suggests an optimal pore diameter in the range between ~4 and 8 Å.[30] The value of 4 Å agrees with the kinetic diameter of SO_2 (4.1 Å).[65] In this PLD range, one can assume the SO_2 molecule to have dispersive interactions with both ends of the molecule to the surface. Such local optima are known for adsorbent structures where the opposite Connolly surfaces are at a distance of the length of the

https://doi.org/10.1021/acsami.1c06003
ACS Appl. Mater. Interfaces 2021, 13, 29137–29149

adsorbed molecule, which can then simultaneously interact with the accessible surface at its opposite sides.[57] Grand-canonical-Monte Carlo (GCMC) simulations for a series of small-pore MOFs have shown a good correlation between the SO_2 uptake at reduced pressures (0.05 bar) and the heat of adsorption.[66]

A pore width of ~4 Å between the Connolly surfaces, i.e., the distance between probe-accessible surfaces of the opposite pore sides[57] allows the SO_2 molecule to have optimal multi-side dispersive interactions. The optimum range up to ~8 Å = 2 × 4 Å can be rationalized through the side-by-side interactions of two adjacent SO_2 molecules through (framework-)O═S···O═S═O(-framework) dipole−dipole interactions. The drop in the surface-specific uptake at larger pore sizes above 8 Å is then due to a change to "one-sided" interactions for the adsorbed SO_2 molecules with the uptake of further SO_2 molecules occurring solely through (framework-)O═S···O═S═O dipole−dipole interactions.[67] MOF-808 shows a somewhat low surface-specific SO_2 uptake at 0.1 bar, but, at an even smaller pressure of 0.01 bar, it has comparable good performance as Al-Fum (Figure S36).

From the conclusion that SO_2 will be preferentially adsorbed in the smallest pores at low pressures, one can also assume the micropore volume or the micropore surface area as the normalizing denominator for the surface-specific SO_2 uptake vs the PLD. The micropore surface area normalization is given in Figures S37 and S38 (at 0.1 and 0.01 bar, respectively). This SO_2 uptake normalization, however, then overenhances the uptake of the two amino-functionalized MOFs, NH_2-MIL-53(Al) and NH_2-MIL-101(Al). Thereby, the importance of amino groups is demonstrated at the same time. Yet, the very small micropore surface area of the largely mesoporous NH_2-MIL-101(Al) gives a small value in the denominator upon normalization, which together with the high uptake of NH_2-MIL-101(Al) then leads to an overall high SO_2 uptake even with the large PLD of about 25 Å (Figures S37 and S38). This would distort the conclusions drawn with respect to PLD.

In summary, the SO_2 adsorption isotherms of typical Zr- and Al-MOFs (Figures 2 and 3 for a combination, see Figure S34) show a wide range of shapes and uptake values in the relevant pressure regions. Once again, we note that a total SO_2 uptake at 1 bar, here found between ~5 and 17 mmol·g^{-1} at 293 K, is less meaningful when aiming for an application in SO_2 separation processes where SO_2 represents only a small volume fraction (<1000 ppm) of the gas mixture. Instead, the noted low-pressure uptake up to ~0.1 bar is more important.

IAST Selectivity. The ideal adsorbed solution theory (IAST) model is a method that gives first estimations on the mixed gas adsorption behavior of an adsorbent based on data gained from single-gas adsorption experiments. IAST-based estimations are most suitable when the following conditions are fulfilled: (i) the same accessible surface area is available to all adsorbates, (ii) low pressures (≤1 bar), and (iii) similar polarity of adsorbates.[68] IAST selectivities in this work were calculated with the "3P sim" software (see the Supporting Information) by fitting the adsorption isotherm data points with the dual-site Langmuir Sips model (DSLS) (Figures S39−S50). Parameters are given in Table S2.

CO_2 can be regarded as the main competitor to SO_2 for a potential adsorptive separation during flue gas desulfurization. IAST selectivities for SO_2/CO_2 gas mixtures for selected MOFs are displayed in Figure 6 (see Table 1 and Figure S51 for all MOFs).

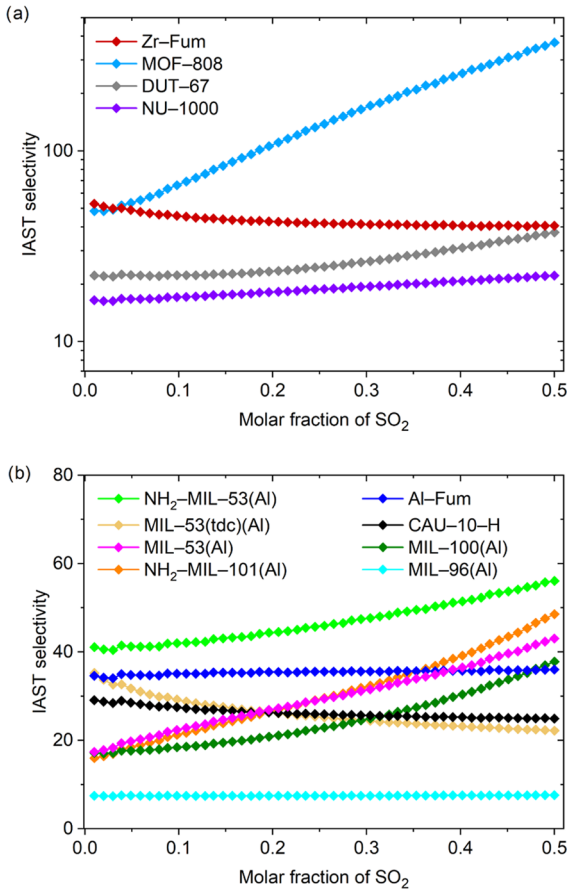

Figure 6. Calculated SO_2/CO_2 IAST selectivity dependence on the molar fraction of SO_2 in the range of 0.01−0.5 at 293 K and 1 bar: (a) Zr-MOFs and (b) Al-MOFs.

The highest calculated SO_2/CO_2 IAST selectivities at 1 bar and low SO_2 mol fraction of 0.01 (1% or 10.000 ppm SO_2) were 53, 48, 41, and 34 for Zr-Fum, MOF-808, NH_2-MIL-53(Al), and Al-Fum, respectively (Table 1). These MOFs had all shown an early steep SO_2 uptake (Figures 2b and 3d), which is one understandable prerequisite for a high SO_2/CO_2 IAST selectivity at a low molar fraction of SO_2 together with a low CO_2 uptake at low pressure (see Table S4).

Isosteric Enthalpy of Adsorption. The isosteric enthalpy of adsorption (ΔH_{ads}) for SO_2 was determined for the representative MOFs, Zr-Fum, Al-Fum, and NH_2-MIL-53(Al), by applying a virial analysis on adsorption isotherm data measured between 293 and 303 K (Figure 7; for details see Section S6.2). The isosteric enthalpy of adsorption near zero coverage (ΔH^0_{ads}) in Zr-Fum is −49 kJ mol^{-1}, whereas Al-Fum and NH_2-MIL-53(Al) exhibit values of −42 and −67 kJ mol^{-1}, respectively. At maximum loading, ΔH_{ads} decreases to −16, −30, and −58 kJ mol^{-1} for Zr-Fum, Al-Fum, and NH_2-MIL-53(Al), respectively. The values of ΔH^0_{ads} can be compared with the DFT-calculated highest binding energies (see below). For Zr-Fum and Al-Fum, the ΔH^0_{ads} value is of the same order of magnitude as in the previously investigated Zr-MOFs (−48 and −51 kJ mol^{-1} for MFM-600[64] and NU-1000,[52] respectively) and Al-MOFs (−42 and −42.8 kJ mol^{-1} for MIL-160[36] and CAU-10-H,[58] respectively). The overall higher adsorption enthalpy for NH_2-MIL-53(Al) can be explained by the strong interaction of the amino group with the polarizable SO_2 molecule.

https://doi.org/10.1021/acsami.1c06003
ACS Appl. Mater. Interfaces 2021, 13, 29137−29149

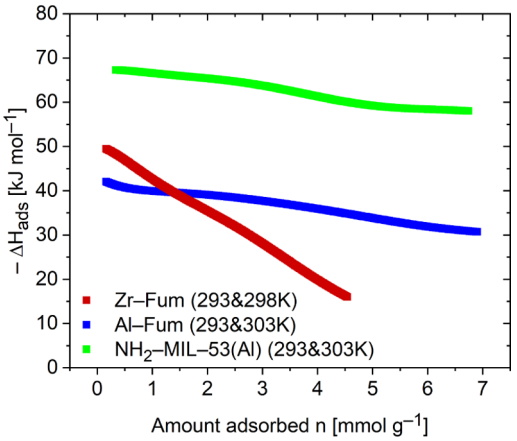

Figure 7. Isosteric enthalpy of adsorption of SO_2 for Zr-Fum, Al-Fum, and NH_2-MIL-53(Al) determined by virial analysis applied on SO_2 adsorption isotherm data measured at temperatures between 293 and 303 K. Computational details are given in the Supporting Information, Section S7.2.

Stability Test toward Dry and Moist SO_2. FGD materials must endure harsh conditions of humid SO_2, containing the moderately strong and quite corrosive sulfurous acid in equilibrium. Though MOFs are often stable toward dry SO_2, many of them degrade when moisture is present.[59] Also, the presence of water could partially shift the adsorption of SO_2 from physisorption to weak chemisorption, which impacts the regeneration of an adsorbent.[11] Therefore, in this study, we tested the stability of all materials after both dry and humid SO_2 exposure conditions (Section S3). To assess the stability, the changes of the PXRD patterns (Figures S10–S21) were examined qualitatively, while changes of the BET-surface area and the total pore volume after exposure were used as the primary quantitative parameters (Figures S22–S33 and 8). It is worth mentioning that distinct changes in the PXRD pattern, after dry or humid SO_2 exposure, were rarely observed. More significant and indicative of framework degradation were losses in surface area for some MOFs. Hence, a combination of diffraction and adsorption experiments is always recommended. Moreover, we note that the distinction between framework degradation and irreversible adsorption is not trivial. However, in materials with potential applicability for FGD, neither framework degradation nor irreversible SO_2 adsorption is preferable. An overview of the results from BET-surface analyses and accessible pore volume, by relating treated/pristine samples, is presented in Figure 8.

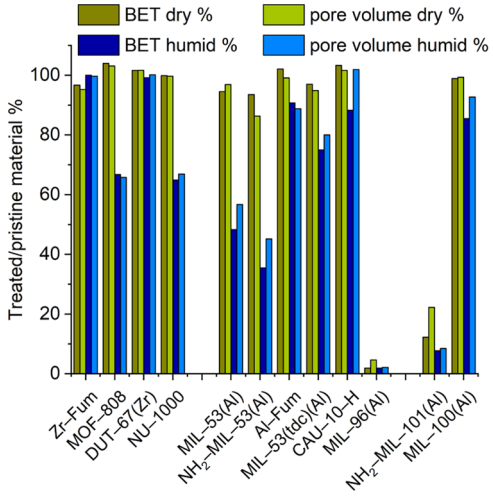

Figure 8. Relative (treated/pristine) BET-surface area and total pore volume of investigated MOFs after dry and humid SO_2 exposure.

Under dry SO_2 exposure, NH_2-MIL-100(Al) and MIL-96(Al) had already demonstrated a major loss of porosity, and thus were deemed SO_2-unstable. Interestingly, the dry SO_2 exposure during ≤10 h did not strongly affect the majority of examined materials (≥90% retained BET-surface area and pore volume). In contrast, under humid SO_2 exposure during 5 h, most MOFs showed a noticeable decrease in accessible porosity. After humid SO_2 exposure, the surface areas of MIL-53(Al) and NH_2-MIL-53(Al) decreased by more than 50%, while NU-1000, MOF-808, Al-Fum, MIL-53(tdc), CAU-10-H, and MIL-100(Al) showed less significant losses in surface area (≥50−90% retained BET-surface area and pore volume). Only Zr-Fum and DUT-67(Zr) showed good performance in both stability tests without a noticeable decrease in porosity. Both MOFs previously showed good water stability also under acidic conditions.[40,69]

DFT Calculations. For the investigation and illustration of the possible binding sites of SO_2, we applied dispersion-corrected DFT (DFT-D) calculations on model frameworks of the three example MOFs—Zr-Fum, Al-Fum, and NH_2-MIL-53(Al). Distances between the oxygen atom of the SO_2 molecule and hydrogen atoms of the framework above 2.8 Å[70] were not viewed as (O/C−)H···O bonds, as the distances between the SO_2 sulfur atom and oxygen atoms of the MOF were above 4 Å. For computational details, see Section S7.

Zr-Fum. With the discrete secondary building units in Zr-Fum, a cluster approach is appropriate. To mimic the local pore environment in Zr-Fum, three different cluster models, each being neutral, were isolated from its crystal structure (Figure 9).

Hydroxido-Centered Model 1. An isolated $[Zr_6(\mu_3\text{-}O)(\mu_3\text{-}OH)(Hfum)_3(O_2CH)_9]$ cluster with three mono-deprotonated fumarate^{1-} ligands surrounding a μ_3-OH group by spanning the three edges of a triangular face of the Zr_6 octahedron was used to model part of the pore cavity (Figure 9a). Out of the 12 bridging fumarate^{2-} ligands around a Zr_6 cluster in Zr-Fum, nine ligands were replaced by formiate ligands, $^{-}O_2CH$, each spanning a Zr···Zr edge of the Zr_6 octahedron. This ensured the electroneutrality of the cluster model.

Metal-Centered Model 2. An isolated $[Zr_6(\mu_3\text{-}O)(\mu_3\text{-}OH)(Hfum)_4(O_2CH)_8]$ cluster with four fumarate^{1-} ligands surrounding a metal vertex by spanning the four edges around a Zr corner of the Zr_6 octahedron was used (Figure 9b).

Oxido-Centered Model 3. The $[Zr_6(\mu_3\text{-}O)(\mu_3\text{-}OH)(Hfum)_3(O_2CH)_9]$ cluster is similar to model 1, except that the three fumarate^{1-} ligands now surround a μ_3-O group (Figure 9c,d).

Four main binding sites for SO_2 are found in the optimized cluster models of Zr-Fum (Figure 9). In binding site 1 of the hydroxido-centered model 1, the O atom of SO_2 interacts with the H atom of the μ_3-OH group. This $OH^{\delta+}\cdots{}^{\delta-}OS$ hydrogen bonding interaction with the optimized H···O distance of 1.88 Å is supplemented by an electrostatic interaction at a distance of 3.33 Å between the fum-carboxylate O atom and the $^{\delta+}$S atom of SO_2 as well as (fum)C···S dispersion interactions. This site has the highest binding energy of −51.5 kJ mol^{-1} of all found four higher-energy binding sites. The value is close to the experimental enthalpy of adsorption near zero coverage

https://doi.org/10.1021/acsami.1c06003
ACS Appl. Mater. Interfaces 2021, 13, 29137−29149

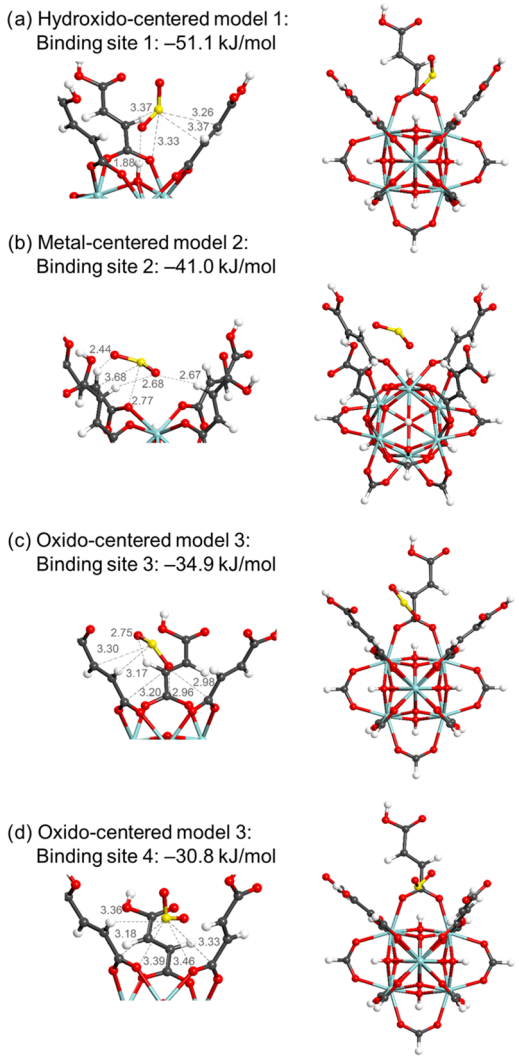

Figure 9. DFT-simulated higher-energy binding sites of SO_2 in Zr-Fum. Left: Close-up of potential SO_2 binding sites with closest contacts (in Å) between the SO_2 molecule to nearby framework atoms depicted by dashed lines. Right: Complete cluster model of SO_2 in Zr-Fum. See the text for a description of models 1−3.

(ΔH^0_{ads}) in Zr-Fum of −49 kJ mol^{-1} (cf. Figure 7). In binding site 2 of the metal-centered model 2, there are multiple weak (fum)CH$^{\delta+}$··· $^{\delta-}$OS interactions (2.44−2.67 Å) together with the electronic attraction between CO$^{\delta-}$···$^{\delta+}$S (2.77 Å), as well as the fum···SO_2 dispersion interactions. Together, this gives site 2 a binding energy of −41.0 kJ mol^{-1}. The next lower-energy binding sites 3 and 4 exist in the oxido-centered model 3. Their lower binding energies of −34.9 and −30.9 kJ mol^{-1}, compared to sites 1 and 2, derive from a longer/weaker (fum)CH$^{\delta+}$···$^{\delta-}$OS contact of 2.75 Å (site 3) and longer/weaker CO$^{\delta-}$···$^{\delta+}$S contacts of 3.39−3.46 Å (site 4) as well as weaker (fum)C···S dispersion interactions than seen for sites 1 and 2, respectively.

Al-MOFs. For Al-Fum and NH_2-MIL-53(Al), with their infinite secondary building units {Al(μ-OH)(O_2C-)$_2$}$_n$, unit cells were generated from their respective crystal structures instead of a cluster model as in Zr-Fum. Figures S56 and S57 depict geometries and structure parameters of the plane wave DFT-D3-optimized Al-MOFs. The free optimized structures exhibit near-parallel alignment of the linker units with 90° O−Al−O angles, while the constrained structures are slightly more distorted. In the constrained structures, the parameters were fixed according to the crystal structure data. We also note variations in the optimized cell vector lengths and angles with respect to the crystal structure parameters. In Al-Fum, the *b*-vector lengthens by ca 0.9 Å, while the respective *a*- and *c*-vectors shorten by 0.1 and 0.2 Å. The β-angle widens by ca. 5°. For NH_2-MIL-53(Al), we observe a lengthening in the *b*- and *a*-vectors of ca. 0.5 and 0.15 Å, respectively, and a shortening of 0.3 Å in the *c*-vector. The overall cell volume is mostly preserved in the optimized vacuum structure of Al-Fum. NH_2-MIL-53(Al) has a ca. 3% larger cell size after full relaxation. Optimization of a single SO_2 molecule within the structures partially results in further contraction along the *c*-axis in Al-Fum and additional lengthening along *b* in NH_2-MIL-53(Al), indicating the breathing capability of both MOFs at low pressures (Figures 10 and 11). Interestingly, most of the computed high-energy binding modes (1−3) show this contraction along *c* and expansion along *b*.

The predominant noncovalent binding mode in sites 1−4 in Al-Fum (Figure 10a−e) can be traced to OH$^{\delta+}$···$^{\delta-}$OS hydrogen bonding interactions of SO_2 with the μ-OH bridge and H···O distances from 1.98 to 2.82 Å. The binding site 1 (Figure 10a) with −51.1 kJ mol^{-1} and with the shortest H···O distance is energetically close to binding sites 2 (−49.5 kJ mol^{-1}) and 3 (−48.6 kJ mol^{-1}). In the latter two sites, the small pores of Al-Fum allow the interaction of two μ-OH bridges from the opposite pore walls with the same SO_2 molecule via OH $^{\delta+}$···$^{\delta-}$OSO$^{\delta-}$···$^{\delta+}$HO hydrogen bonds (Figure 10b,c). The experimental enthalpy of adsorption near zero coverage (ΔH^0_{ads}) in Al-Fum was −42 kJ mol^{-1} (cf. Figure 7).

In the two lower-energy binding sites 4a and 4b of equal energy (−41.0 kJ mol^{-1}), again SO_2 interacts with the framework through OH$^{\delta+}$···$^{\delta-}$OS and a (fum)CH$^{\delta+}$···$^{\delta-}$OS hydrogen bond in site 4a, while weaker H···O hydrogen bonding is observed in site 4b (Figure 10d,e). Additional (fum)CO$^{\delta-}$···$^{\delta+}$$SO_2$ contacts as well as (fum)C···OSO dispersion interactions lead to the energy differentiation between the binding sites in Figure 10.

From the fully relaxed optimization of NH_2-MIL-53(Al) with one SO_2 molecule, we obtained at least four binding sites with binding energies ranging from −67.3 to −49.1 kJ mol^{-1} (Figure 11a−d). Binding site 1 (Figure 11a) has the highest binding energy (−67.3 kJ mol^{-1}), and it is dominated by NH$^{\delta+}$···$^{\delta-}$OS hydrogen bonding and HN$^{\delta-}$···$^{\delta+}$SO electrostatic attractive interactions between −NH_2 groups from two independent BDC-NH_2 linkers. The value is again close to the experimental enthalpy of adsorption near zero coverage (ΔH^0_{ads}) in NH_2-MIL-53(Al) of −67 kJ mol^{-1} (cf. Figure 7). Binding site 2 (Figure 11b) has a slightly lower binding energy (−58.2 kJ mol^{-1}). Here, SO_2 mainly binds to C_6-π from bdc-NH_2 through C_6-$\pi^{\delta-}$···$^{\delta+}$SO interactions with C_6-π···S distances between 2.99 and 3.19 Å. For binding site 3 (Figure 11c) with a binding energy of −55.1 kJ mol^{-1}, we note a NH$^{\delta+}$···$^{\delta-}$OS hydrogen bond, COO$^{\delta-}$···$^{\delta+}$SO electrostatic interactions, and weak CH$^{\delta+}$···$^{\delta-}$OS interactions as cooperating effects, trapping SO_2 within the pores of NH_2-MIL-53(Al). The shortest distances between SO_2 and the ligands (NH$^{\delta+}$···$^{\delta-}$OS = 1.99 Å and CH$^{\delta+}$···$^{\delta-}$OS = 2.56 Å) in site 3 are between ligands on different Al atoms. Binding site 4 (Figure 11d) has the lowest binding energy (−49.1 kJ mol^{-1}); besides C6-$\pi^{\delta-}$···$^{\delta+}$SO and NH$^{\delta+}$···$^{\delta-}$OS interactions, an additional OH$^{\delta+}$···$^{\delta-}$OS hydrogen bond between μ-OH and SO_2 contributes to the adsorption of SO_2.

https://doi.org/10.1021/acsami.1c06003
ACS Appl. Mater. Interfaces 2021, 13, 29137−29149

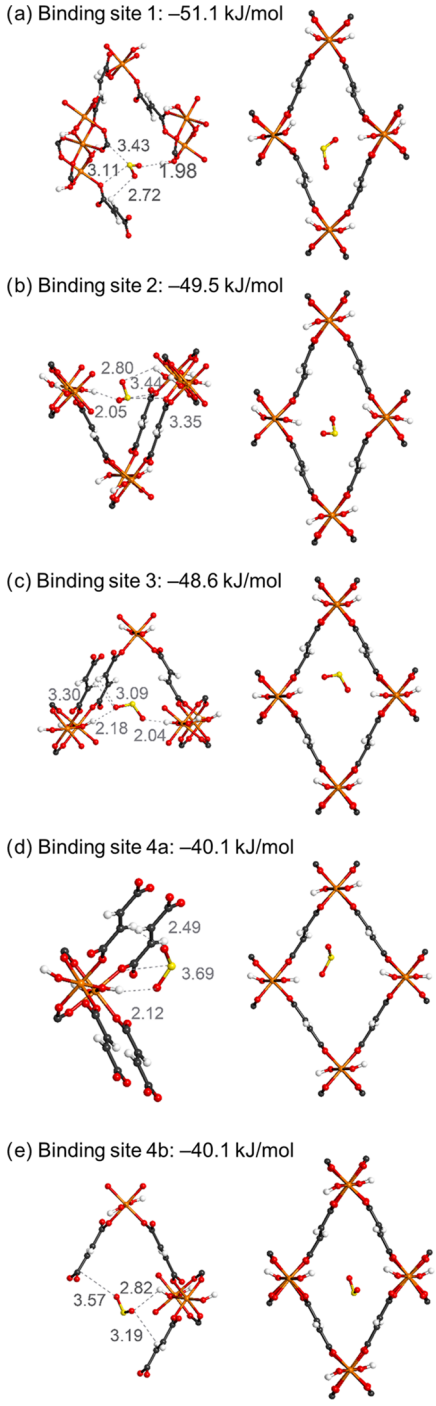

Figure 10. DFT-simulated higher-energy binding sites of SO_2 in Al-Fum. Left: Close-up of potential SO_2 binding sites with closest contacts (in Å) between the SO_2 molecule to nearby framework atoms depicted by dashed lines. Right: Cross-sectional model of SO_2 in Al-Fum. See the text for a description of the model.

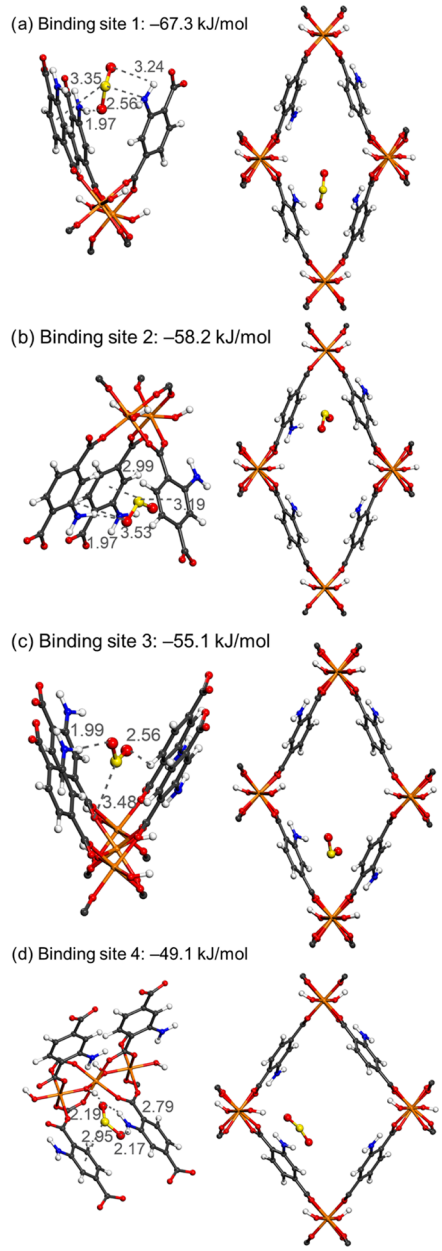

Figure 11. DFT-simulated higher-energy binding sites of SO_2 in NH_2-MIL-53(Al). Left: Close-up of potential SO_2 binding sites with closest contacts in Å between the SO_2 molecule to nearby framework atoms depicted by dashed lines. Right: Cross-sectional model of SO_2 in NH_2-MIL-53(Al). See the text for a description of the model.

It should be noted that the free relaxation of Al-Fum and NH_2-MIL-53(Al) cells for each binding site can give an additional contribution to the binding energy.

Further, we simulated SO_2 adsorption isotherms for Al-Fum in the pressure range of 0.01−1 bar at 293 K (Figure S58) using the GCMC program Cassandra (for computational details, see Section S7.3). The simulations were performed using either a fully relaxed geometry or the fixed cell parameters of the crystal structure data and by setting the Lennard-Jones parameter ε for aluminum either to 254.12 K (100%) or zero, allowing only electrostatic interactions with this atom type. The best agreement with our experimental data was achieved with the fixed geometry and ε(Al) = 0, which somewhat underestimated the SO_2 adsorption capability or with the approach using the relaxed structure and ε(Al) = 100%, which overestimated the SO_2 adsorption capability of Al-Fum.

The simulated isotherm data for Al-Fum was also used to model the pore filling in Al-Fum by a GCMC approach and is displayed in the form of single snapshots related to a defined pressure or as a movie, with a time-lapse over the complete pressure range (Figure S59 and Supporting Movies: SI-Al-Fum-2 kPa and SI-Al-Fum-0.05−100 kPa). Within the snapshots (e.g., at 2 and 3 kPa), it is observed that some pores are empty,

https://doi.org/10.1021/acsami.1c06003
ACS Appl. Mater. Interfaces 2021, 13, 29137−29149

while nearby pores are already filled with multiple SO_2 molecules. This could be an indication of uneven filling of the pores, which might be caused by intermolecular dipole−dipole interactions of the SO_2 adsorptive process. It is recognized that the dipole moment of SO_2 plays an important role in the adsorption process with the pore filling occurring by (framework-)O═S···O═S═O and (framework-)O═S═O···S═O dipole−dipole interactions, forming SO_2 chains or clusters. However, this observation could also be assigned to "artifacts/background noise" of the randomized Monte-Carlo simulations and thus needs further investigations.

CONCLUSIONS

Four Zr- and eight Al-MOFs, most of which are frequently investigated prototypical MOFs, were examined for their SO_2 adsorption capability to identify factors that influence the activity of SO_2 separations from CO_2 by MOFs. A strong correlation between the SO_2 uptake and BET-surface area and pore volume, at 1 bar and 293 K, was observed for all materials independent of their pore structure. Especially, MOFs featuring narrow pores with pore diameters between ∼4 and 8 Å yielded high SO_2 affinities.

Also, amino groups at the linker tend to be advantageous for tuning SO_2 affinity. Among all tested MOFs, NH_2-MIL-53(Al), which combines both of the aforementioned properties, showed the highest SO_2 affinity and excellent low-pressure adsorption performance.

The chemical stability of MOFs vs acidic gases such as SO_2 over a prolonged time (10 h) and in the presence of moisture (for 5 h) presents a fundamental problem. Among the selected and proven water-stable Zr- and Al-MOFs, only Zr-Fum and DUT-67(Zr) could be called stable, while the other MOFs showed more or less loss of porosity, especially under the simultaneous presence of SO_2 and H_2O. Interestingly, PXRD patterns were less indicative of framework degradation than losses in surface area (porosity). This suggests that degradation at the pore mouths leads to pore blocking, thereby leaving the inner framework of the MOF crystallites intact, albeit inaccessible.

Theoretical calculations on Zr-Fum, Al-Fum, and NH_2-MIL-53(Al) point also to metal-bridging μ-OH- and NH_2-groups in the SBU or at the linker as an important component of primary binding sites for $-OH^{\delta+}\cdots^{\delta-}OSO$ and $-NH^{\delta+}\cdots^{\delta-}OSO$ hydrogen bonding interactions with binding energies of −50 kJ mol^{-1} and above. At the same time, a low CO_2 affinity is required for trace SO_2 separation from flue gases. Calculated IAST selectivities for the highly SO_2-affine MOFs, Zr-Fum, MOF-808, NH_2-MIL-53(Al), reached values above 40 for SO_2/CO_2 binary gas mixtures and low SO_2 mol fraction of 0.01 (1% or 10.000 ppm SO_2) at 1 bar.

In the end, this work not only gives a compilation of potential MOFs for possible use in adsorptive flue gas desulfurization processes but also offers guidelines to design new adsorbents for this important application.

ASSOCIATED CONTENT

Supporting Information

The Supporting Information is available free of charge at https://pubs.acs.org/doi/10.1021/acsami.1c06003.

Synthesis of MOFs; additional MOF structure figures; powder X-ray diffractograms; gas sorption isotherms and measurement details; isotherm fitting and simulation parameters; details on DFT and GCMC calculations and simulations; and comparison of SO_2 sorption literature data (PDF)

SI-Al-Fum-2 kPa (Movie) (MP4)

SI-Al-Fum-0.05−100 kPa (Movie) (MP4)

AUTHOR INFORMATION

Corresponding Authors

Oliver Weingart − *Institut für Theoretische Chemie und Computerchemie, Heinrich-Heine-Universität Düsseldorf, 40225 Düsseldorf, Germany*; Email: oliver.weingart@hhu.de

Christoph Janiak − *Institut für Anorganische Chemie und Strukturchemie, Heinrich-Heine-Universität Düsseldorf, 40225 Düsseldorf, Germany; Hoffmann Institute of Advanced Materials, Shenzhen Polytechnic, Shenzhen 518055, China*; orcid.org/0000-0002-6288-9605; Email: janiak@hhu.de

Authors

Philipp Brandt − *Institut für Anorganische Chemie und Strukturchemie, Heinrich-Heine-Universität Düsseldorf, 40225 Düsseldorf, Germany*

Shang-Hua Xing − *Institut für Anorganische Chemie und Strukturchemie, Heinrich-Heine-Universität Düsseldorf, 40225 Düsseldorf, Germany; Hoffmann Institute of Advanced Materials, Shenzhen Polytechnic, Shenzhen 518055, China*

Jun Liang − *Institut für Anorganische Chemie und Strukturchemie, Heinrich-Heine-Universität Düsseldorf, 40225 Düsseldorf, Germany; Hoffmann Institute of Advanced Materials, Shenzhen Polytechnic, Shenzhen 518055, China*

Gülin Kurt − *Institut für Anorganische Chemie und Strukturchemie, Heinrich-Heine-Universität Düsseldorf, 40225 Düsseldorf, Germany*

Alexander Nuhnen − *Institut für Anorganische Chemie und Strukturchemie, Heinrich-Heine-Universität Düsseldorf, 40225 Düsseldorf, Germany*

Complete contact information is available at: https://pubs.acs.org/10.1021/acsami.1c06003

Notes

The authors declare no competing financial interest.

ACKNOWLEDGMENTS

The authors thank Dr. István Boldog for constructive discussions and his overall support. This work was supported by the Deutsche Forschungsgemeinschaft (DFG)—396890929/GRK 2482.

REFERENCES

(1) Várhelyi, G. Continental and Global Sulfur Budgets-I. Anthropogenic SO_2 Emissions. *Atmos. Environ.* **1985**, *19*, 1029−1049.

(2) International Energy Agency. *World Energy Outlook 2019*; OECD Publishing: Paris, 2019.

(3) Likens, G. E.; Driscoll, C. T.; Buso, D. C. Long-Term Effects of Acid Rain: Response and Recovery of a Forest Ecosystem. *Science* **1996**, *272*, 244−246.

(4) Gregory, K.; Webster, C.; Durk, S. Estimates of Damage to Forests in Europe due to Emissions of Acidifying Pollutants. *Energy Policy* **1996**, *24*, 655−664.

(5) Reiss, R.; Anderson, E. L.; Cross, C. E.; Hidy, G.; Hoel, D.; McClellan, R.; Moolgavkar, S. Evidence of health impacts of sulfate-and nitrate-containing particles in ambient air. *Inhalation Toxicol.* **2007**, *19*, 419−449.

(6) Srivastava, R. K.; Jozewicz, W. Flue Gas Desulfurization: The State of the Art. *J. Air Waste Manage. Assoc.* **2001**, *51*, 1676−1688.

(7) Rao, A. B.; Rubin, E. S. A Technical, Economic, and Environmental Assessment of Amine-Based CO_2 Capture Technology for Power Plant Greenhouse Gas Control. *Environ. Sci. Technol.* **2002**, *36*, 4467−4475.
(8) Ding, S.; Liu, F.; Shi, X.; Liu, K.; Lian, Z.; Xie, L.; He, H. Significant Promotion Effect of Mo Additive on a Novel Ce−Zr Mixed Oxide Catalyst for the Selective Catalytic Reduction of NO_x with NH_3. *ACS Appl. Mater. Interfaces* **2015**, *7*, 9497−9506.
(9) Goo, J. H.; Irfan, M. F.; Kim, S. D.; Hong, S. C. Effects of NO_2 and SO_2 on Selective Catalytic Reduction of Nitrogen Oxides by Ammonia. *Chemosphere* **2007**, *67*, 718−723.
(10) Kohl, A. L.; Nielsen, R. *Gas Purification*; Gulf Professional: Houston, TX, 1997.
(11) Hanif, M. A.; Ibrahim, N.; Abdul Jalil, A. Sulfur Dioxide Removal: An Overview of Regenerative Flue Gas Desulfurization and Factors affecting Desulfurization Capacity and Sorbent Regeneration. *Environ. Sci. Pollut. Res.* **2020**, *27*, 27515−27540.
(12) Evans, J. D.; Garai, B.; Reinsch, H.; Li, W.; Dissegna, S.; Bon, V.; Senkovska, I.; Fischer, R. A.; Kaskel, S.; Janiak, C.; Stock, N.; Volkmer, D. Metal−organic frameworks in Germany: From synthesis to function. *Coord. Chem. Rev.* **2019**, *380*, 378−418.
(13) Suh, M. P.; Park, H. J.; Prasad, T. K.; Lim, D. W. Hydrogen Storage in Metal Organic Frameworks. *Chem. Rev.* **2012**, *112*, 782−835.
(14) Sumida, K.; Rogow, D. L.; Mason, J. A.; McDonald, T. M.; Bloch, E. D.; Herm, Z. R.; Bae, T.-H.; Long, J. R. Carbon Dioxide Capture in Metal-Organic Frameworks. *Chem. Rev.* **2012**, *112*, 724−781.
(15) He, Y.; Zhou, W.; Qian, G.; Chen, B. Methane Storage in Metal-Organic Frameworks. *Chem. Soc. Rev.* **2014**, *43*, 5657−5678.
(16) Britt, D.; Tranchemontagne, D.; Yaghi, O. M. Metal-Organic Frameworks with High Capacity and Selectivity for Harmful Gases. *Proc. Natl. Acad. Sci. U.S.A.* **2008**, *105*, 11623−11627.
(17) Bobbitt, N. S.; Mendonca, M. L.; Howarth, A. J.; Islamoglu, T.; Hupp, J. T.; Farha, O. K.; Snurr, R. Q. Metal-Organic Frameworks for the Removal of Toxic Industrial Chemicals and Chemical Warfare Agents. *Chem. Soc. Rev.* **2017**, *46*, 3357−3385.
(18) Wang, H.; Lustig, W. P.; Li, J. Sensing and Capture of Toxic and Hazardous Gases and Vapors by Metal-Organic Frameworks. *Chem. Soc. Rev.* **2018**, *47*, 4729−4756.
(19) Han, X.; Yang, S.; Schröder, M. Porous Metal-Organic Frameworks as Emerging Sorbents for Clean Air. *Nat. Rev. Chem.* **2019**, *3*, 108−118.
(20) Jurado-Vázquez, T.; Sánchez-González, E.; Campos-Reales-Pineda, A. E.; Islas-Jácome, A.; Lima, E.; González-Zamora, E.; Ibarra, I. A. MFM-300: From Air Pollution Remediation to Toxic Gas Detection. *Polyhedron* **2019**, *157*, 495−504.
(21) Martínez-Ahumada, E.; López-Olvera, A.; Jancik, V.; Sánchez-Bautista, J. E.; González-Zamora, E.; Martis, V.; Williams, D. R.; Ibarra, I. A. MOF Materials for the Capture of Highly Toxic H_2S and SO_2. *Organometallics* **2020**, *39*, 883−915.
(22) Islamoglu, T.; Chen, Z.; Wasson, M. C.; Buru, C. T.; Kirlikovali, K. O.; Afrin, U.; Mian, M. R.; Farha, O. K. Metal-Organic Frameworks against Toxic Chemicals. *Chem. Rev.* **2020**, *120*, 8130−8160.
(23) Fernandez, C. A.; Thallapally, P. K.; Motkuri, R. K.; Nune, S. K.; Sumrak, J. C.; Tian, J.; Liu, J. Gas-Induced Expansion and Contraction of a Fluorinated Metal−Organic Framework. *Cryst. Growth Des.* **2010**, *10*, 1037−1039.
(24) Thallapally, P. K.; Motkuri, R. K.; Fernandez, C. A.; McGrail, B. P.; Behrooz, G. S. Prussian Blue Analogues for CO_2 and SO_2 Capture and Separation Applications. *Inorg. Chem.* **2010**, *49*, 4909−4915.
(25) Glover, T. G.; Peterson, G. W.; Schindler, B. J.; Britt, D.; Yaghi, O. MOF-74 Building Unit has a Direct Impact on Toxic Gas Adsorption. *Chem. Eng. Sci.* **2011**, *66*, 163−170.
(26) Tan, K.; Canepa, P.; Gong, Q.; Liu, J.; Johnson, D. H.; Dyevoich, A.; Thallapally, P. K.; Thonhauser, T.; Li, J.; Chabal, Y. J. Mechanism of Preferential Adsorption of SO_2 into Two Microporous Paddle Wheel Frameworks $M(bdc)(ted)_{0.5}$. *Chem. Mater.* **2013**, *25*, 4653−4662.
(27) Tchalala, M. R.; Bhatt, P. M.; Chappanda, K. N.; Tavares, S. R.; Adil, K.; Belmabkhout, Y.; Shkurenko, A.; Cadiau, A.; Heymans, N.; Weireld, G.; Maurin, G.; Salama, K. N.; Eddaoudi, M. Fluorinated MOF Platform for Selective Removal and Sensing of SO_2 from Flue Gas and Air. *Nat. Commun.* **2019**, *10*, No. 1328.
(28) Zárate, J. A.; Sánchez-González, E.; Williams, D. R.; González-Zamora, E.; Martis, V.; Martínez, A.; Balmaseda, J.; Maurin, G.; Ibarra, I. A. High and Energy-Efficient Reversible SO_2 Uptake by a Robust Sc(III)-Based MOF. *J. Mater. Chem. A* **2019**, *7*, 15580−15584.
(29) Domínguez-González, R.; Rojas-León, I.; Martínez-Ahumada, E.; Martínez-Otero, D.; Lara-García, H. A.; Balmaseda-Era, J.; Ibarra, I. A.; Percástegui, E. G.; Jancik, V. UNAM-1: A Robust Cu I and Cu II Containing 3D-hydrogen-Bonded Framework with Permanent Porosity and Reversible SO_2 Sorption. *J. Mater. Chem. A* **2019**, *7*, 26812−26817.
(30) Zhang, Y.; Zhang, P.; Yu, W.; Zhang, J.; Huang, J.; Wang, J.; Xu, M.; Deng, Q.; Zeng, Z.; Deng, S. Highly Selective and Reversible Sulfur Dioxide Adsorption on a Microporous Metal-Organic Framework via Polar Sites. *ACS Appl. Mater. Interfaces* **2019**, *11*, 10680−10688.
(31) Walton, I.; Chen, C.; Rimsza, J. M.; Nenoff, T. M.; Walton, K. S. Enhanced Sulfur Dioxide Adsorption in UiO-66 Through Crystal Engineering and Chalcogen Bonding. *Cryst. Growth Des.* **2020**, *20*, 6139−6146.
(32) Chen, Z.; Wang, X.; Cao, R.; Idrees, K. B.; Liu, X.; Wasson, M. C.; Farha, O. K. Water-Based Synthesis of a Stable Iron-Based Metal−Organic Framework for Capturing Toxic Gases. *ACS Mater. Lett.* **2020**, *2*, 1129−1134.
(33) Yang, S.; Sun, J.; Ramirez-Cuesta, A. J.; Callear, S. K.; David, W. I. F.; Anderson, D. P.; Newby, R.; Blake, A. J.; Parker, J. E.; Tang, C. C.; Schröder, M. Selectivity and Direct Visualization of Carbon Dioxide and Sulfur Dioxide in a Decorated Porous Host. *Nat. Chem.* **2012**, *4*, 887−894.
(34) Carter, J.; Morris, C.; Godfrey, H. G. W.; Day, S. J.; Potter, J.; Thompson, S. P.; Tang, C.; Yang, S.; Schröder, M. Long-Term Stability of MFM-300(Al) Towards Toxic Air Pollutants. *ACS Appl. Mater. Interfaces* **2020**, *12*, 42949−42954.
(35) Carter, J. H.; Han, X.; Moreau, F. Y.; da Silva, I.; Nevin, A.; Godfrey, H. G. W.; Tang, C. C.; Yang, S.; Schröder, M. Exceptional Adsorption and Binding of Sulfur Dioxide in a Robust Zirconium-Based Metal-Organic Framework. *J. Am. Chem. Soc.* **2018**, *140*, 15564−15567.
(36) Brandt, P.; Nuhnen, A.; Lange, M.; Möllmer, J.; Weingart, O.; Janiak, C. Metal−Organic Frameworks with Potential Application for SO_2 Separation and Flue Gas Desulfurization. *ACS Appl. Mater. Interfaces* **2019**, *11*, 17350−17358.
(37) Brandt, P.; Nuhnen, A.; Öztürk, S.; Kurt, G.; Liang, J.; Janiak, C. Comparative Evaluation of Different MOF and Non-MOF Porous Materials for SO_2 Adsorption and Separation Showing the Importance of Small Pore Diameters for Low-Pressure Uptake. *Adv. Sustainable Syst.* **2021**, *5*, No. 2000285.
(38) Low, J. J.; Benin, A. I.; Jakubczak, P.; Abrahamian, J. F.; Faheem, S. A.; Willis, R. R. Virtual high throughput screening confirmed experimentally: porous coordination polymer hydration. *J. Am. Chem. Soc.* **2009**, *131*, 15834−15842.
(39) Sun, Y.; Spieß, A.; Jansen, C.; Nuhnen, A.; Gökpinar, S.; Wiedey, R.; Ernst, S.-J.; Janiak, C. Tunable LiCl@UiO-66 composites for water sorption-based heat transformation applications. *J. Mater. Chem. A* **2020**, *8*, 13364−13375.
(40) Burtch, N. C.; Jasuja, H.; Walton, K. S. Water Stability and Adsorption in Metal-Organic Frameworks. *Chem. Rev.* **2014**, *114*, 10575−10612.
(41) Ding, M.; Cai, X.; Jiang, H.-L. Improving MOF Stability: Approaches and Applications. *Chem. Sci.* **2019**, *10*, 10209−10230.
(42) Furukawa, H.; Gándara, F.; Zhang, Y.-B.; Jiang, J.; Queen, W. L.; Hudson, M. R.; Yaghi, O. M. Water Adsorption in Porous Metal-Organic Frameworks and Related Materials. *J. Am. Chem. Soc.* **2014**, *136*, 4369−4381.
(43) Islamoglu, T.; Otake, K.-i.; Li, P.; Buru, C. T.; Peters, A. W.; Akpinar, I.; Garibay, S. J.; Farha, O. K. Revisiting the Structural Homogeneity of NU-1000, a Zr-Based Metal−Organic Framework. *CrystEngComm* **2018**, *20*, 5913−5918.
(44) Loiseau, T.; Serre, C.; Huguenard, C.; Fink, G.; Taulelle, F.; Henry, M.; Bataille, T.; Férey, G. A Rationale for the Large Breathing of

the Porous Aluminum Terephthalate (MIL-53) Upon Hydration. *Chem. – Eur. J.* **2004**, *10*, 1373–1382.
(45) Gascon, J.; Aktay, U.; Hernandezalonso, M.; Vanklink, G.; Kapteijn, F. Amino-Based Metal-Organic Frameworks as Stable, Highly Active Basic Catalysts. *J. Catal.* **2009**, *261*, 75–87.
(46) Alvarez, E.; Guillou, N.; Martineau, C.; Bueken, B.; Van de Voorde, B.; Le Guillouzer, C.; Fabry, P.; Nouar, F.; Taulelle, F.; de Vos, D.; Chang, J. S.; Cho, K. H.; Ramsahey, N.; Devic, T.; Daturi, M.; Maurin, G.; Serre, C. The Structure of the Aluminum Fumarate Metal-Organic Framework A520. *Angew. Chem.* **2015**, *127*, 3735–3739.
(47) Tschense, C. B. L.; Reimer, N.; Hsu, C.-W.; Reinsch, H.; Siegel, R.; Chen, W.-J.; Lin, C.-H.; Cadiau, A.; Serre, C.; Senker, J.; Stock, N. New Group 13 MIL-53 Derivates based on 2,5-Thiophenedicarboxylic Acid. *Z. Anorg. Allg. Chem.* **2017**, *643*, 1600–1608.
(48) Teo, H. W. B.; Chakraborty, A. Water Adsorption on Various Metal Organic Frameworks. *IOP Conf. Ser.: Mater. Sci. Eng.* **2017**, *272*, No. 012019.
(49) Benzaqui, M.; Pillai, R. S.; Sabetghadam, A.; Benoit, V.; Normand, P.; Marrot, J.; Menguy, N.; Montero, D.; Shepard, W.; Tissot, A.; Martineau-Corcos, C.; Sicard, C.; Mihaylov, M.; Carn, F.; Beurroies, I.; Llewellyn, P. L.; De Weireld, G.; Hadjiivanov, K.; Gascon, J.; Kapteijn, F.; Maurin, G.; Stenou, N.; Serre, C. Revisiting the Aluminum Trimesate-Based MOF (MIL-96): From Structure Determination to the Processing of Mixed Matrix Membranes for CO_2 Capture. *Chem. Mater.* **2017**, *29*, 10326–10338.
(50) Jeremias, F.; Khutia, A.; Henninger, S. K.; Janiak, C. MIL-100(Al, Fe) as water adsorbents for heat transformation purposes—a promising application. *J. Mater. Chem.* **2012**, *22*, 10148–10151.
(51) Navarro-Sánchez, J.; Almora-Barrios, N.; Lerma-Berlanga, B.; Ruiz-Pernía, J. J.; Lorenz-Fonfria, V. A.; Tuñón, I.; Martí-Gastaldo, C. Translocation of Enzymes into a Mesoporous MOF for Enhanced Catalytic Activity under Extreme Conditions. *Chem. Sci.* **2019**, *10*, 4082–4088.
(52) Gorla, S.; Díaz-Ramírez, M. L.; Abeynayake, N. S.; Kaphan, D. M.; Williams, D. R.; Martis, V.; Lara-García, H. A.; Donnadieu, B.; Lopez, N.; Ibarra, I. A.; Montiel-Palma, V. Functionalized NU-1000 with an Iridium Organometallic Fragment: SO_2 Capture Enhancement. *ACS Appl. Mater. Interfaces* **2020**, *12*, 41758–41764.
(53) Mouchaham, G.; Wang, S.; Serre, C. The Stability of Metal-Organic Frameworks. In *Metal-Organic Frameworks: Applications in Separations and Catalysis*; García, H.; Navalon, S., Eds.; Wiley-VCH: Weinheim, 2018.
(54) Alhamami, M.; Doan, H.; Cheng, C.-H. A Review on Breathing Behaviors of Metal-Organic-Frameworks (MOFs) for Gas Adsorption. *Materials* **2014**, *7*, 3198–3250.
(55) Loiseau, T.; Lecroq, L.; Volkringer, C.; Marrot, J.; Férey, G.; Haouas, M.; Taulelle, F.; Bourrelly, S.; Llewellyn, P. L.; Latroche, M. MIL-96, a Porous Aluminum Trimesate 3D Structure Constructed from a Hexagonal Network of 18-Membered Rings and μ_3-Oxo-Centered Trinuclear Units. *J. Am. Chem. Soc.* **2006**, *128*, 10223–10230.
(56) Li, J.; Zhou, Z.; Han, X.; Zhang, X.; Yan, Y.; Li, W.; Smith, G. L.; Cheng, Y.; McCormick McPherson, L. J.; Teat, S. J.; Frogley, M. D.; Rudić, S.; Ramirez-Cuesta, A. J.; Blake, A. J.; Sun, J.; Schröder, M.; Yang, S. Guest-Controlled Incommensurate Modulation in a Meta-Rigid Metal-Organic Framework Material. *J. Am. Chem. Soc.* **2020**, *142*, 19189–19197.
(57) Thommes, M.; Kaneko, K.; Neimark, A. V.; Olivier, J. P.; Rodriguez-Reinoso, F.; Rouquerol, J.; Sing, K. S. W. Physisorption of gases, with special reference to the evaluation of surface area and pore size distribution (IUPAC Technical Report). *Pure Appl. Chem.* **2015**, *87*, 1051–1069.
(58) Zárate, J. A.; Domínguez-Ojeda, E.; Sánchez-González, E.; Martínez-Ahumada, E.; López-Cervantes, V. B.; Williams, D. R.; Martis, V.; Ibarra, I. A.; Alejandre, J. Reversible and Efficient SO_2 Capture by a Chemically stable MOF CAU-10: Experiments and Simulations. *Dalton Trans.* **2020**, *49*, 9203–9207.
(59) Mounfield, W. P.; Han, C.; Pang, S. H.; Tumuluri, U.; Jiao, Y.; Bhattacharyya, S.; Dutzer, M. R.; Nair, S.; Wu, Z.; Lively, R. P.; Sholl, D. S.; Walton, S. W. Synergistic Effects of Water and SO_2 on Degradation of MIL-125 in the Presence of Acid Gases. *J. Phys. Chem. C* **2016**, *120*, 27230–27240.
(60) Li, Z.; Liao, F.; Jiang, F.; Liu, B.; Ban, S.; Chen, G.; Sun, C.; Xiao, P.; Sun, Y. Capture of H_2S and SO_2 from trace sulfur containing gas mixture by functionalized UiO-66(Zr) materials: A molecular simulation study. *Fluid Phase Equilib.* **2016**, *427*, 259–267.
(61) Zhang, Z.; Yang, B.; Ma, H. Aliphatic amine decorating metal–organic framework for durable SO_2 capture from flue gas. *Sep. Purif. Technol.* **2021**, *259*, No. 118164.
(62) Martínez-Ahumada, E.; Díaz-Ramírez, M. L.; Lara-García, H. A.; Williams, D. R.; Martis, V.; Jancik, V.; Lima, E.; Ibarra, I. A. High and Reversible SO_2 Capture by a Chemically Stable Cr(III)-Based MOF. *J. Mater. Chem. A* **2020**, *8*, 11515–11520.
(63) Liu, J.-X.; Li, J.; Tao, W.-Q.; Li, Z. 3. Al-Based Metal-Organic Framework MFM-300 and MIL-160 for SO_2 Capture: A Molecular Simulation Study. *Fluid Phase Equilib.* **2021**, *536*, No. 112963.
(64) Carter, J. H.; Han, X.; Moreau, F. Y.; da Silva, I.; Nevin, A.; Godfrey, H. G. W.; Tang, C. C.; Yang, S.; Schröder, M. Exceptional Adsorption and Binding of Sulfur Dioxide in a Robust Zirconium-Based Metal–Organic Framework. *J. Am. Chem. Soc.* **2018**, *140*, 15564–15567.
(65) Li, J.-R.; Kuppler, R. J.; Zhou, H.-C. Selective Gas Adsorption and Separation in Metal-Organic Frameworks. *Chem. Soc. Rev.* **2009**, *38*, 1477–1504.
(66) Song, X.-D.; Wang, S.; Hao, C.; Qiu, J.-S. Investigation of SO_2 Gas Adsorption in Metal–Organic Frameworks by Molecular Simulation. *Inorg. Chem. Commun.* **2014**, *46*, 277–281.
(67) Lowell, S.; Shields, J. E.; Thomas, M. A.; Thommes, M. Adsorption Isotherms. In *Characterization of Porous Solids and Powders: Surface Area, Pore Size and Density*; Springer International Publishing: Cham, 2004; pp 11–14.
(68) Cessford, N. F.; Seaton, N. A.; Düren, T. Evaluation of Ideal Adsorbed Solution Theory as a Tool for the Design of Metal-Organic Framework Materials. *Ind. Eng. Chem. Res.* **2012**, *51*, 4911–4921.
(69) Bon, V.; Senkovska, I.; Evans, J. D.; Wöllner, M.; Hölzel, M.; Kaskel, S. Insights into the Water Adsorption Mechanism in the Chemically Stable Zirconium-Based MOF DUT-67 – a Prospective Material for Adsorption-Driven Heat Transformations. *J. Mater. Chem. A* **2019**, *7*, 12681–12690.
(70) Desiraju, G. R.; Steiner, T. The Weak Hydrogen Bond. In *IUCr Monograph on Crystallography*; Oxford Science: Oxford, 1999; Vol. *9*.

https://doi.org/10.1021/acsami.1c06003
ACS Appl. Mater. Interfaces 2021, 13, 29137–29149